

## On the dynamics of twinning in magnesium micropillars

Kristián Máthis<sup>a</sup>, Michal Knapek<sup>a,b,\*</sup>, Filip Šiška<sup>c</sup>, Petr Harcuba<sup>a</sup>, Dávid Ugi<sup>d</sup>, Péter Dusán Ispánovity<sup>d</sup>, István Groma<sup>d</sup>, Kwang Seon Shin<sup>e</sup>

<sup>a</sup> Charles University, Faculty of Mathematics and Physics, Department of Physics of Materials, Ke Karlovu 5, 12116 Prague 2, Czech Republic

<sup>b</sup> Nuclear Physics Institute of the Czech Academy of Sciences, Husinec – Řež 130, 25068 Řež, Czech Republic

<sup>c</sup> Institute of Physics of Materials of the Czech Academy of Sciences, CEITEC-IPM, Žitkova 22, 61600 Brno, Czech Republic

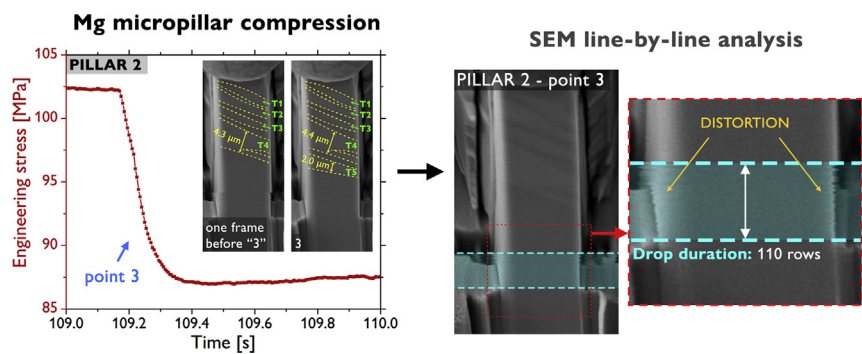
<sup>d</sup> Loránd Eötvös University, Department of Materials Physics, Pázmány Péter sétány 1/a, 1117 Budapest, Hungary

<sup>e</sup> Seoul National University, Magnesium Technology Innovation Center, School of Materials Science and Engineering, Gwanak-gu, Seoul 151-744, Republic of Korea

### HIGHLIGHTS

- Single-crystal Mg micropillars ( $10 \times 10 \times 30 \mu\text{m}^3$ ) favorably oriented for mechanical twinning were tested in compression.
- High-precision compression data and in-situ SEM observation were supplemented by finite element modeling.
- Gradual nucleation of twins from top to bottom across the micropillar was observed, followed by their subsequent thickening.
- The existence of critical width (around  $3 \mu\text{m}$  here) was proved responsible for such nucleation and growth dynamics.
- Detailed examination of SEM images and stress drops indicated twin lateral growth rates on the order of  $10^{-5}$ – $10^{-4}$  m/s.

### GRAPHICAL ABSTRACT



### ARTICLE INFO

#### Article history:

Received 15 December 2020

Received in revised form 26 January 2021

Accepted 4 February 2021

Available online 13 February 2021

#### Keywords:

Magnesium

Micropillar

Compression

Twinning

Finite element modeling

Scanning electron microscopy

### ABSTRACT

Micro-deformation testing has recently gained far-reaching scientific importance as it provides intrinsic information on the dynamics of plastic deformation which is concealed when bulk materials are tested. In this work, single-crystal Mg micropillars favorably oriented for mechanical twinning were tested in compression with concurrent scanning electron microscopy imaging. The experimental data were complemented by the finite element modeling in order to reveal the underlying physical background of the observed twinning dynamics. It was shown that the thickness of a twin should reach a critical value before triggering the nucleation of another twin to accommodate further strain. Nucleation and growth are repeated until the twins form throughout the whole micropillar, from top to bottom. Afterwards, the thickening and coalescence of all these twins take place until the entire micropillar volume is twinned. In addition, a line-by-line analysis of the scanning electron microscopy images was employed to reveal the twin lateral growth rates, which were shown to be on the order of  $10^{-5}$ – $10^{-4}$  m/s.

© 2021 The Author(s). Published by Elsevier Ltd. This is an open access article under the CC BY-NC-ND license (<http://creativecommons.org/licenses/by-nc-nd/4.0/>).

\* Corresponding author at: Charles University, Faculty of Mathematics and Physics, Department of Physics of Materials, Ke Karlovu 5, 12116 Prague 2, Czech Republic.

E-mail address: [knapek@karlov.mff.cuni.cz](mailto:knapek@karlov.mff.cuni.cz) (M. Knapek).

## 1. Introduction

The investigation of deformation mechanisms in magnesium alloys has always been a challenging task. Owing to their hexagonal-closed-packed structure, concurrent activation of several dislocation slip systems and deformation twinning can take place. The particular scenario of the plastic flow is strongly influenced by various microstructural (e.g. grain size [1] and texture [2]) and experimental (e.g. testing temperature [3,4] and strain path [5,6]) parameters. Consequently, there is a high demand in the scientific community for experimental techniques, which enable studying the operation of particular mechanisms individually. The micrometer-scale deformation testing fulfills these requirements [7–11]. Moreover, such tests are indispensable in the development of modern micro-/nano-electromechanical devices (MEMS/NEMS), as at small scales, the deformation behavior becomes less predictable [12,13].

Unlike bulk deformation testing, where the discrete dynamics of lattice defects typically cancel out, micro-testing techniques provide essential insights into the intrinsic intermittent character of plastic flow [11,14]. Usually, such studies involve nanoindenter compression of micropillars with diameters/widths between 0.1 and 10  $\mu\text{m}$ . However, for magnesium, only a limited number of micropillar studies are available. The so-called size effect (i.e. the inverse dependence of strength on micropillar cross-section) has been the most investigated physical phenomenon [9,14–17]. Some works have focused on the investigation of discontinuous plastic flow for Mg micropillar orientations facilitating the activity of multiple deformation mechanisms (e.g. the combination of dislocation slip and twinning) [6,18,19]. Pure Mg micropillars were tested in tension by Della Ventura et al. [20] for orientations where both dislocation slip and twinning occurred, and the influence of the activity of different slip systems on the twin nucleation and propagation was studied. The extension twinning was investigated in Mg micropillars, where the  $(0\bar{1}12)$  plane was perpendicular to the loading direction [18,21]. In such a case, the basal slip also becomes active in the twinned area in the latter stages of loading. Micropillars with the  $[10\bar{1}0]$  orientation, i.e. having the Schmid factor of extension twinning of 0.5, were investigated in compression by Liu et al. [7], focusing on the quantification of the critical resolved shear stresses (CRSS) associated with basal slip and twinning. Related studies on the  $[10\bar{1}0]$  orientation have also been published recently by Wang [22] and Ma [6], with particular focus on the effect of Al solutes content on CRSS values and twinning dynamics in Mg–Al micropillars. The studies which focus primarily on the in-situ monitoring of twinning dynamics in pure Mg are, however, very scarce. Moreover, there is no general code-of-practice for micropillar testing, which often obscures the comparison of the results from different authors. Cylindrical micropillar specimens are typically tapered, which causes uneven stress concentrations, these being the highest within the upper part of micropillars [23,24]. Moreover, certain types of indentation devices cannot handle the massive stress drops taking place during loading, resulting in repeated unloading of the specimen [7,18,22]. Hence, the associated relaxation effects make it difficult to follow twinning dynamics properly.

In this work, we present the results on compression testing of pure magnesium micropillars with the  $[10\bar{1}0]$  orientation, i.e. ideally oriented for the  $\{10\bar{1}2\}\{10\bar{1}1\}$ -type extension twinning. With this orientation, no dislocation slip is expected to occur up to several percent of strain even in the twinned areas [7], thus enabling us to effectively monitor extension twinning evolution without the influence of other deformation mechanisms. Several reports showed that for Mg micropillars, there is a breakdown in the size-dependent plasticity if the micropillar cross-section becomes larger than several micrometers [7,17,25]. Specifically, Liu et al. [7] showed that a minimum micropillar diameter required to obtain yield strength similar to that of bulk Mg single

crystal is  $\sim 10 \mu\text{m}$ . For this reason, micropillars with a rectangular cross-section of  $10 \mu\text{m}$  were fabricated, which could be effectively tested in-situ using the micro-testing device inside the scanning electron microscope (SEM) chamber and, at the same time, should be representative enough of bulk deformation behavior. A custom-made micropillar tester, having high spatial and force resolution, together with a novel pillar fabrication process, were used in order to fully exploit the potential of in-situ SEM testing. The paper provides a comprehensive description of the twinning dynamics in Mg micropillars, including autocatalytic twin nucleation and twin boundary movement rates determined by SEM imaging. Furthermore, a 3D finite element (FE) model was used for revealing the driving forces for twin nucleation and thickening.

## 2. Experimental

A small block having the surface normal of  $[10\bar{1}0]$  was cut from the Mg single crystal (99.99 wt% Mg) by a spark erosion device. The rectangular micropillars with the dimension of  $10 \times 10 \times 30 \mu\text{m}^3$  were fabricated at the edge of the oriented single crystal block by focused ion beam (FIB) milling with a Ga ion source. Using this fabrication technique, the inclination of the lateral side of the micropillars was negligible ( $< 0.5^\circ$ ). The shape and position of pillars very close to the edge of the sample also allowed easy and precise characterization of crystallographic orientation of the pillars by means of EBSD both before and after the test. The micromechanical compression tests were performed using an in-house built nano-testing device [26]. The specimen was mounted on a stage enabling positioning in the X and Y directions using the linear ultrasonic motors. In the Z direction, two stages are used: (i) a linear step-motor stage for “raw” movement of the indenter towards the sample and (ii) a piezoelectric positioning (PEP) stage with a resolution of  $\sim 0.1 \text{ nm}$ . During the actual compression test, only the precise PEP stage is being moved. A standard spring with high transversal but very low longitudinal stiffness is mounted on the PEP stage for the recording of external force. During the compression test, the PEP stage moves at a constant rate. The force and the sample deformation are determined as follows. Concurrently with the Z direction movement  $d$  of the PEP stage (to which the diamond-tip indenter is attached), the elongation  $e$  of the spring is also measured by a capacitive sensor. The sample deformation is then expressed as  $\varepsilon = d - e$  and the acting force as  $F = ke$ , where  $k$  is the stiffness of the spring (for further details, see Hegyi et al. [26]).

Two micropillars were tested at an initial crosshead speed (i.e. the PEP stage movement) of  $0.01 \mu\text{m/s}$ . The compression was realized by using a boron-doped flat punch diamond tip connected to a spring. The first pillar was twin free (further referred to as P1) and in the second one (referred to as P2), three small twins were present in the initial state near the diamond indenter tip, caused by touching the pillar by the indenter before the test (i.e. these twins were not present in the material before micropillar preparation). The measured displacement data were corrected for the compliance of the pillar base. The surface of the micropillars during the deformation was monitored continuously with a sampling frequency of 2 fps (pillar 1) or 1 fps (pillar 2), using the FEI Quanta 3D SEM.

### 2.1. FE simulations

The experiments were supported by numerical simulations to reveal local phenomena that play roles in the observed deformation mechanisms. These simulations were performed using a finite element method (FEM) within the framework of crystal plasticity. The FE model constitutes 3D representation of a micropillar with already fully grown twins inside. Variants of the model include situations with 1 twin with different thickness ( $t = 1.5, 3, 4.5$  and  $6 \mu\text{m}$  – 4 variants) and with 2 twins with equal thicknesses ( $t = 3$  or  $4.5 \mu\text{m}$ ) and mutual

distance ( $d = 1.5, 3, 4.5$  and  $6 \mu\text{m}$ ) giving 8 different variants. The twin geometry corresponds to  $\{10\bar{1}2\}$  twin orientation. Matrix and twin areas have different crystallographic orientations corresponding to experimental observations. Analysis of twin shear stress fields induced in these cases can show the effect of twins' thickness and their mutual position on further twin growth and/or further twin nucleation.

The FE model was created in the FE code Z-set and represents half of the pillar due to the symmetry conditions (i.e.  $10 \times 5 \times 30 \mu\text{m}$ ). The boundary conditions were chosen to closely correspond to the experimental set-up. The boundary conditions at the surface representing the micropillar interior were prescribed such that they represented the symmetry conditions. The load was applied by the displacement of the upper face of the pillar. The rest of the surfaces were traction-free. The mesh consisted of 18,260 quadratic elements (C3D20). The constitutive behavior is based on anisotropic elasticity and crystal plasticity, which is implemented in the code. Elastic constants representative of magnesium are summarized in Table 1 [27].

The crystal plasticity is based on the decomposition of the deformation gradient into elastic and plastic parts [28,29]:

$$F = F^e F^p \tag{1}$$

where the plastic part is related to the slip occurring in the slip systems characterized by slip direction ( $\mathbf{m}^s$ ) and normal to the slip plane ( $\mathbf{n}^s$ ). It can be written as:

$$\dot{F}^p F^{p-1} = \sum_{s=1}^n \dot{\gamma}^s \mathbf{m}^s \otimes \mathbf{n}^s. \tag{2}$$

Slip rate on a given slip system  $\dot{\gamma}^s$  is defined by the following expression:

$$\dot{\gamma}^s = \left\langle \frac{|\tau^s| - \tau_h^s}{K} \right\rangle^n \text{sign}(\tau^s) \tag{3}$$

where  $\tau^s$  is the resolved shear stress,  $\tau_h^s$  is the corresponding isotropic strain hardening variable. A non-linear hardening rule is prescribed by the following equation:

$$\tau_h^s = \tau_0 + g \sum_{r=1}^n h^{sr} (1 - \exp(-bv^r)). \tag{4}$$

where  $\tau_0$  is the initial value of critical resolved shear stress (CRSS),  $g$  and  $b$  are phenomenological constants,  $v^r$  is the cumulated plastic slip for a system ( $r$ ). Slip systems interaction is described by the hardening matrix  $h^{sr}$ . Its components are equal to 1, so no self or latent hardening is taken into account. Parameters  $K$  and  $n$  were set according to Guillemer et al. [30] and parameters  $\tau_0, g$  and  $b$  were estimated by fitting the experimental stress-strain curves for micropillars with an orientation that favors basal slip. The ratios of prismatic/basal and pyramidal/basal CRSS values were considered to be 2:1 and 4:1, respectively, according to [4]. All parameters of the applied crystal plasticity model are summarized in Table 2.

### 3. Results and discussion

The stress-time compression curves<sup>1</sup> of the tested pillars and the specific points at the curves corresponding to the stress drops are shown in Fig. 1. Fig. 2 shows the pixel intensity evolution in the central part of both pillars, reflecting the occurrence and progression of twins. Fig. 3 displays snapshots at distinctive points as marked in Fig. 1. It is evidenced in Fig. 2 and Fig. 3 that all the large stress drops are explicitly connected to twin nucleation (see also Supplementary animations). Moreover, as the inset of Fig. 1a – presenting the EBSD micrographs

<sup>1</sup> The stress-time representation instead of stress-strain one is preferred here owing to the easier correlation of the SEM pictures and the deformation curves.

**Table 1**  
Magnesium elastic constants used in the simulations [27].

$C_{1111}$ [GPa]	$C_{2222}$ [GPa]	$C_{3333}$ [GPa]	$C_{1212}$ [GPa]	$C_{2323}$ [GPa]	$C_{3131}$ [GPa]	$C_{1122}$ [GPa]	$C_{2233}$ [GPa]	$C_{3311}$ [GPa]
59.7	59.7	61.7	16.8	16.4	16.4	26.2	20.8	20.8

**Table 2**  
Coefficients of the constitutive model.

$K$ [MPa·s]	$N$	$g$ [MPa]	$b$	$h^{sr}$	$\tau_0$ basal [MPa]	$\tau_0$ prismatic [MPa]	$\tau_0$ pyramidal [MPa]
1.0	25.0	28.0	30.0	1.0	11.0	22.0	44.0

before and after the deformation of pillar 1 – also shows, the entire volume became twinned during compression (this matter will be discussed in detail later). It is obvious that during the deformation, several twins formed and coalesced as the strain increased (Fig. 2 and 3). For pillar P1, the first twins nucleated in the stress range of 75–85 MPa, which is in good agreement with the literature data [7,22,25]. Note that the first stress drop in the deformation curve of pillar P1 (Fig. 1) did not give rise to visible changes in the SEM image (Fig. 2 and 3). A rapid movement of the indenter was, however, recorded at this point (see Supplementary animations) and we speculate that a

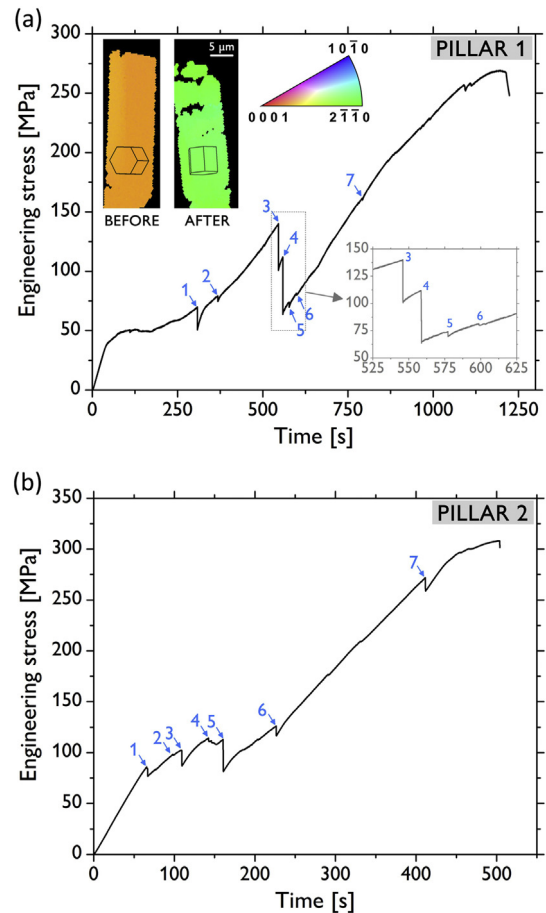


**Fig. 1.** (a) The deformation curve of P1 with highlighted distinctive points corresponding to discernible stress drops; inset 1 - the zoomed-in portion of the curve; inset 2 - the EBSD micrographs of the pillar before and after compression. (b) The deformation curve of P2 with highlighted specific points corresponding to discernible stress drops.

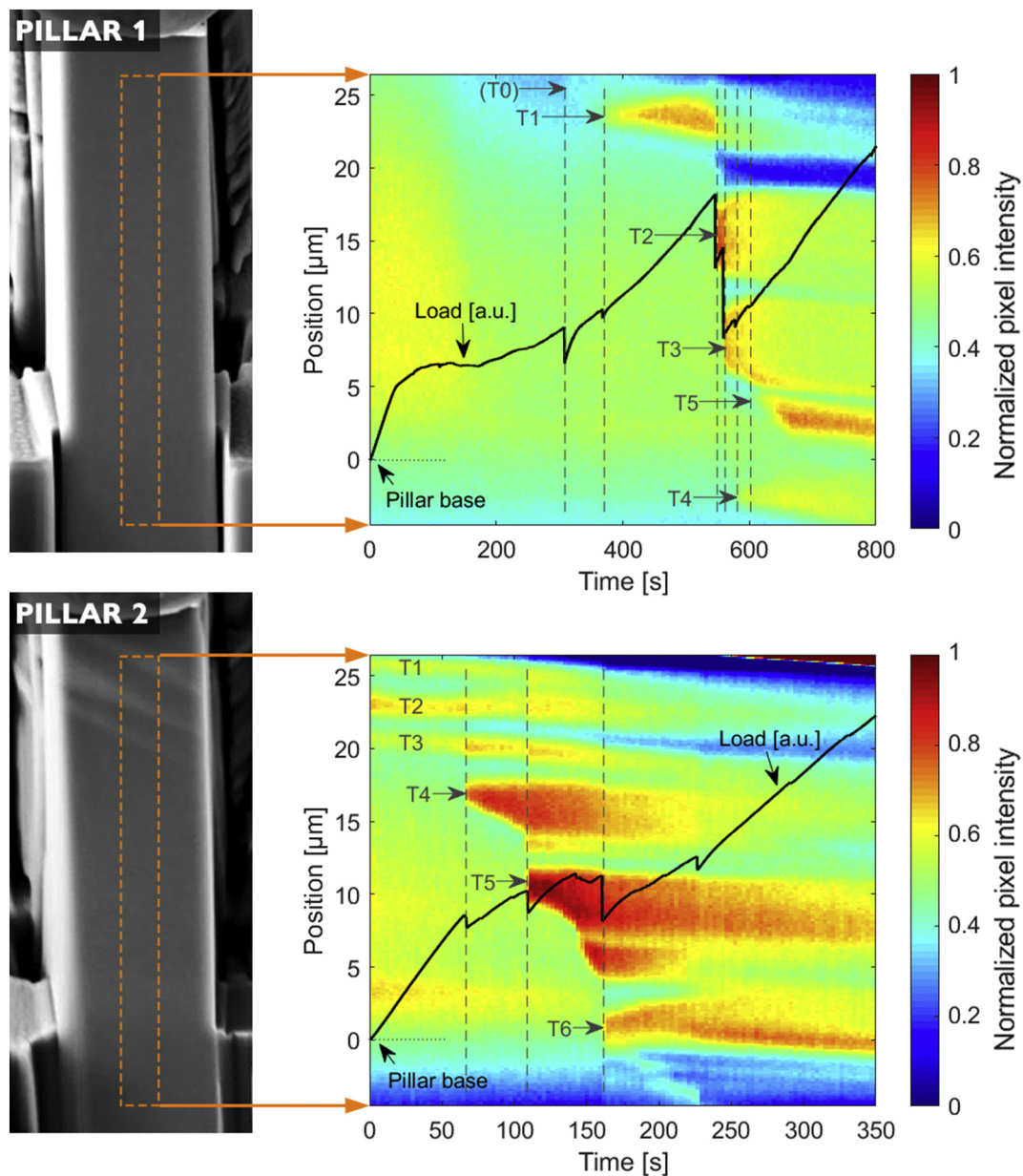


**Fig. 2.** The evolution of normalized average pixel intensity in the central part of both micropillars reflecting the presence and progression of twinning. The width of the analyzed area was 30 px.

small twin (T0) might have nucleated in the rear part of the pillar, possibly related to T1 occurring slightly later. The common feature of the first visible small twin (T1) in pillar P1 and the pre-existing twins (T1, T2, and T3) in pillar P2 was that their thickness remained rather constant during the straining. Such an effect was also observed by Liu et al. [7] and it was ascribed to the large back-stress arising at the twin tip, where the stiff indenter touches the top of the pillar, as will be discussed in detail later. The second twin (T2) in P1 and the first newly nucleated twin (T4) in P2 exhibited rapid nucleation and lateral growth (for the twinning progression dynamics, see also Table 3). These newly nucleated twins were clearly more prone to subsequent thickening than the former ones up to the moment when another twin nucleated below (Fig. 2 and Table 3). These dynamics were characteristic of straining until the twins nucleated along the entire pillar height, i.e. from the top of the pillar down to the pillar base (point 5 for both pillars).

During further straining, all the nucleated twins continuously grew and, finally, they coalesced, accompanied only by sporadic discernible

stress drops (points 6 and 7 for both pillars), which seemed to be related to further twinning activity near the pillar base (this is best seen in the Supplementary material). The details on the growth dynamics of individual twins are effectively tracked in Table 1 and Fig. 2, which further elaborate and confirm an increased thickening tendency for newly nucleated twins. It is worth noting that practically all the twins nucleated within one SEM image (i.e. one “frame”).

In order to explain the nucleation dynamics, with a focus especially on the fact that the twins nucleated successively from the top of the pillar down to its base, the 3D FE modeling was employed. The calculated shear stress distributions in the micropillars containing twins are plotted in Fig. 4. As the compression direction was perpendicular to the plane, the  $\{10\bar{1}2\}$  twin lamellae were inclined by  $46.84^\circ$  with respect to the pillar basal plane. Twin interactions during their growth were modeled by several scenarios containing one or two twins with different thicknesses and distances. Specifically, the twin thicknesses projected to the loading directions were  $1.5\ \mu\text{m}$ ,  $3\ \mu\text{m}$ ,  $4.5\ \mu\text{m}$ , or  $6\ \mu\text{m}$

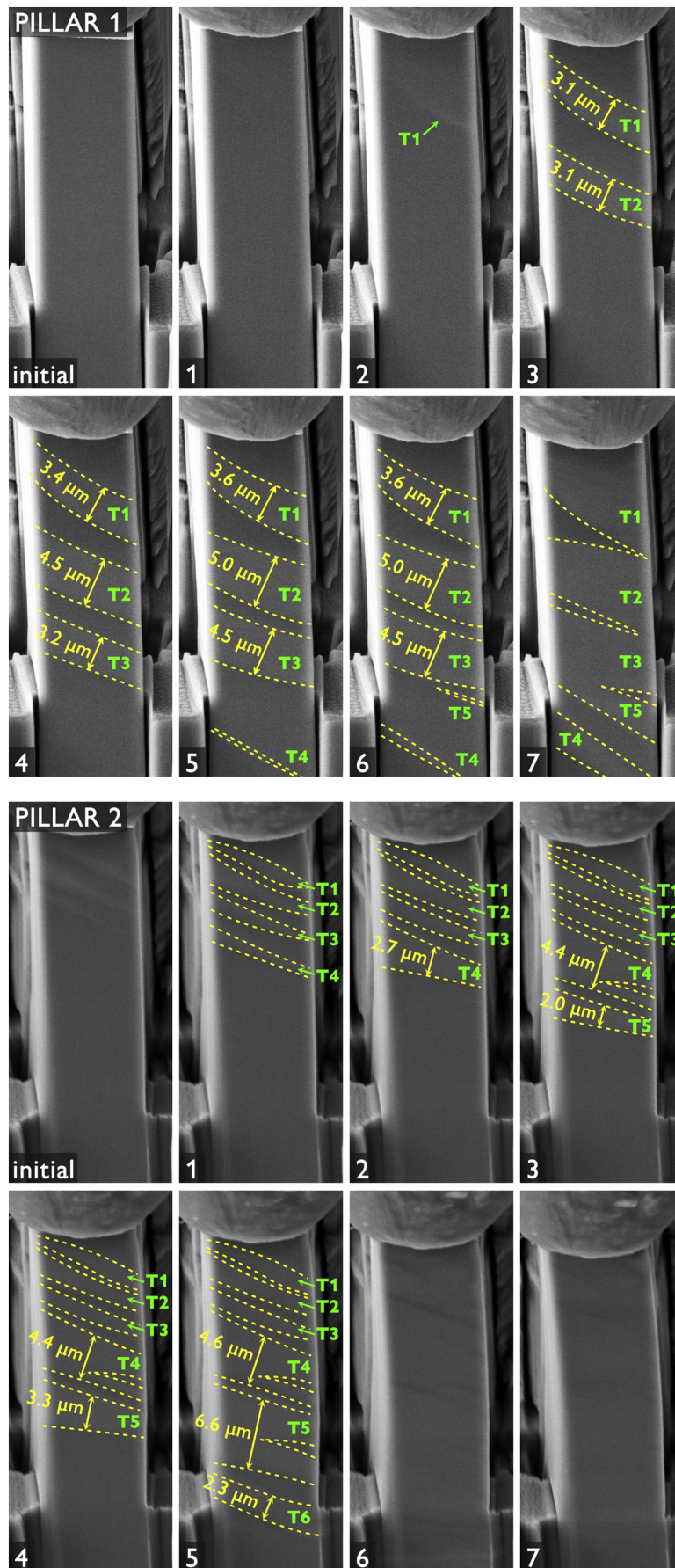


Fig. 3. The twin evolution and growth dynamics of the tested micropillars at the distinctive points during the compression test.

**Table 3**

The nucleation and evolution of twins corresponding to specific stages of the deformation curves (N – nucleation, RG – rapid growth, GG – gradual growth, NC – no change). In the used notation XX/YY, XX represents the behavior during the interval between two points, e.g. 1 → 2 and YY represents the behavior at a particular instance following this interval, e.g. point 2, as denoted in the first row. The reader is advised to see Supplementary animations.

Pillar P1	init→1/1	1 → 2/2	2 → 3/3	3 → 4/4	4 → 5/5	5 → 6/6	6 → 7/7
T1	-/-	-/N	GG/GG	GG/RG	GG/GG	NC/NC	GG/GG
T2	-/-	-/-	-/N	GG/RG	GG/GG	NC/NC	GG/GG
T3	-/-	-/-	-/-	-/N	GG/GG	NC/NC	GG/GG
T4	-/-	-/-	-/-	-/-	-/N	GG/GG	GG/GG
T5	-/-	-/-	-/-	-/-	-/-	-/N	GG/GG
Pillar P2	init→1/1	1 → 2/2	2 → 3/3	3 → 4/4	4 → 5/5	5 → 6/6	6 → 7/7
T1	PE/GG	NC/NC	NC/NC	NC/NC	NC/NC	GG/GG	GG/GG
T2	PE/GG	GG/GG	NC/NC	NC/NC	NC/NC	GG/GG	GG/GG
T3	PE/GG	GG/GG	NC/NC	NC/NC	NC/NC	GG/GG	GG/GG
T4	-/N	GG/GG	GG/GG	NC/NC	GG/GG	GG/GG	GG/GG
T5	-	-	-/N	GG/GG	GG/GG	GG/GG	GG/GG
T6	-	-	-	-	-/N	GG/GG	GG/GG

for the single-twin set-up, and 3  $\mu\text{m}$  and 4.5  $\mu\text{m}$  for the double-twin set-up (representing approximately 10% and 15% of the micropillar volume fraction, respectively) and the distance between the twins was set to 1.5  $\mu\text{m}$ , 3  $\mu\text{m}$ , 4.5  $\mu\text{m}$  or 6  $\mu\text{m}$ .

The presented modeling results describe the stress distribution at an applied strain of 0.0075, at which the twins were already present in the experiments. Note that the stress distributions inside the twins do not provide relevant data for the analysis owing to the different crystallographic orientation of the twin interior. Accordingly, these areas were greyed out in Fig. 4. The stress distribution in the vicinity of the twin-matrix interfaces was quite heterogeneous. High stress concentrations appeared in the matrix near the twin boundaries (Fig. 4a-l) and in the regions between the twins (Fig. 4e-l). The shear stress level in the matrix was about 30–40 MPa, while in the concentration areas near the twin boundaries it could reach up to 60 MPa. These observations must be related to both the twin nucleation and growth. It can be observed in Fig. 4a-d that the stress concentration in the matrix, predominantly in the vicinity of twin boundaries, increases with increasing twin thickness only marginally. Instead, the stress intensity is obviously driven by the level of external load. On the other hand, for the two-twin configurations (Fig. 4e-l) the stress concentration between the twins reaches the highest value when their distance is intermediate (3  $\mu\text{m}$  or 4.5  $\mu\text{m}$ ) while the stress accumulation for the distances of 1  $\mu\text{m}$  and 6  $\mu\text{m}$  is lower. Specifically, Fig. 4e-l shows that the highest stress is achieved when the distance between the twins is close to their thickness.

The correlation of the “static” FEM calculations (Fig. 4) with the “dynamic” SEM experimental data can elucidate the observed autocatalytic twin nucleation and growth dynamics (cf. Fig. 2, Fig. 3 and Supplementary animations). In pillar P1, at the beginning of the straining, twin T1 nucleated close to the pillar top, hence it could not grow much. The respective deformation curve (Fig. 1a) exhibited a rather prompt stress increase after the initial drop related to T1 nucleation, which shows that even though the micropillar accommodates external loading by the twin formation (and possible thickening), additional deformation is required to accommodate further strain, leading to an increase in the overall stress level. Therefore, at a certain instant, the stress concentration below the initial twin reaches the level for a new twin initiation. For this reason and also due to the necessity of further strain accommodation, the subsequent new twin T2, which nucleated at point 3, appeared below (i.e. in the area of stress concentration – cf. Fig. 4a-d) and grew quite rapidly. Similarly, the stress concentration below this twin became large enough for the initiation of a new twin very quickly and after

reaching a critical size of  $\sim 3.1 \mu\text{m}$  it “autocatalytically” triggered the nucleation of T3 (point 4). Owing to the considerable stress concentration, T3 reached the critical width of 3  $\mu\text{m}$  also quite rapidly, leading to the nucleation of T4. As further strain was quite effectively accommodated by twins T1-T4 (i.e. their slow thickening), the dynamics of the occurrence and growth of T5 and T6 were somewhat less swift. In the case of pillar P2, the scenario was quite similar – apart from the existing twins, the new ones nucleated below the last twin after it reached a thickness of  $\sim 3 \mu\text{m}$ . The general observation is, therefore, that the twins in the vicinity of the pillar top grow only slowly and new twins appear gradually below. It should also be noted that as each new twin nucleates, the stress concentration in the newly formed inter-twin region arises, which in most cases leads to some thickening of the adjacent twins, in agreement with Fig. 2 and 3. However, as mentioned above, the stress concentration between the twins is a function of their distance. In the case of both thinner (3  $\mu\text{m}$ ) and thicker (4.5  $\mu\text{m}$ ) twins (Fig. 4e-l) the distance leading to the highest stress concentration is similar to the twin thickness. Increasing or decreasing this twin distance hence results in a decrease in the stress concentration, thus imposing certain bounds for the neighboring twin thickening and, in turn, impeding their complete and instantaneous coalescence. Such an effect is observed only when there is no room left for further twinning at the pillar bottom, resulting in the thickening of all the existing twins and possible activation of additional deformation mechanisms.

We speculate that the effect of uneven shear stress in the horizontal direction is also manifested in the twin shapes. It is evident in Fig. 4 that the stress is somewhat higher on the right side below each twin. In most cases, the twin thickness in the SEM images is either higher near the right edge (T1 and T2 in P1 and T6 in P2 in Fig. 3) or a small new twin nucleates below the twin with a lower right-hand side thickness (twin pairs T3-T5 in P1, and twins T4 and T5 in P2, Fig. 3). With further straining, such twin pairs merge and grow together, leaving behind a small “wedge”. Finally, when there are enough twins across the entire pillar height (P1 – point 6, P2 – point 5 in Fig. 3), the strain starts to be accommodated by their slow thickening driven by stress concentrations near the twin boundaries until the entire volume is twinned. Note that this observation was confirmed by the EBSD observations shown in Fig. 1 and also agrees with the Mg micropillar compression results reported elsewhere [7,22]. It should be noted that no traces of dislocation slip were observed before the entire micropillar was twinned, as expected for the involved  $[10\bar{1}0]$  crystal orientation.

It was shown by Jeong et al. [18] that single-crystal Mg pillars that do not feature pre-existing grain or twin boundaries necessitate different sources for twin nucleation. It was confirmed by transmission electron microscopy (TEM) observations that pile-ups of prismatic  $\langle a \rangle$  dislocation (which are present in abundance, owing to the FIB processing) provide required local stresses for the nucleation of new twins. Liu et al. [7] used full-field elasto-visco-plastic Fast Fourier Transform model [31] to determine the local stress distribution related to twin configurations. The calculations showed a large back-stress induced as a result of the lack of plastic accommodation in the vicinity of the twin top in the presence of a stiff indenter. Hence, the growth of twins closer to the pillar top is limited, which agrees well with our experimental observations as well as with the outcomes of the FE model, even though these approaches differ technically. Elaborating further on these considerations, increased back-stress towards the top of pillars can also explain asymmetric twin growth discussed above: the part of twin further from the indenter is more prone to thickening, or a new twin can nucleate in these areas, as documented in Fig. 2 and 3. Finally, it was demonstrated by the authors in [18] that the decelerating effect of back-stress acting on the growing twin might bring about repeated nucleation of new twin below. In other words, existing twins effectively promote nucleation of new twins in the stress concentration areas in order to accommodate strain, again in accordance with our experimental and modeling data. The twinning dynamics in Mg-based polycrystals were recently

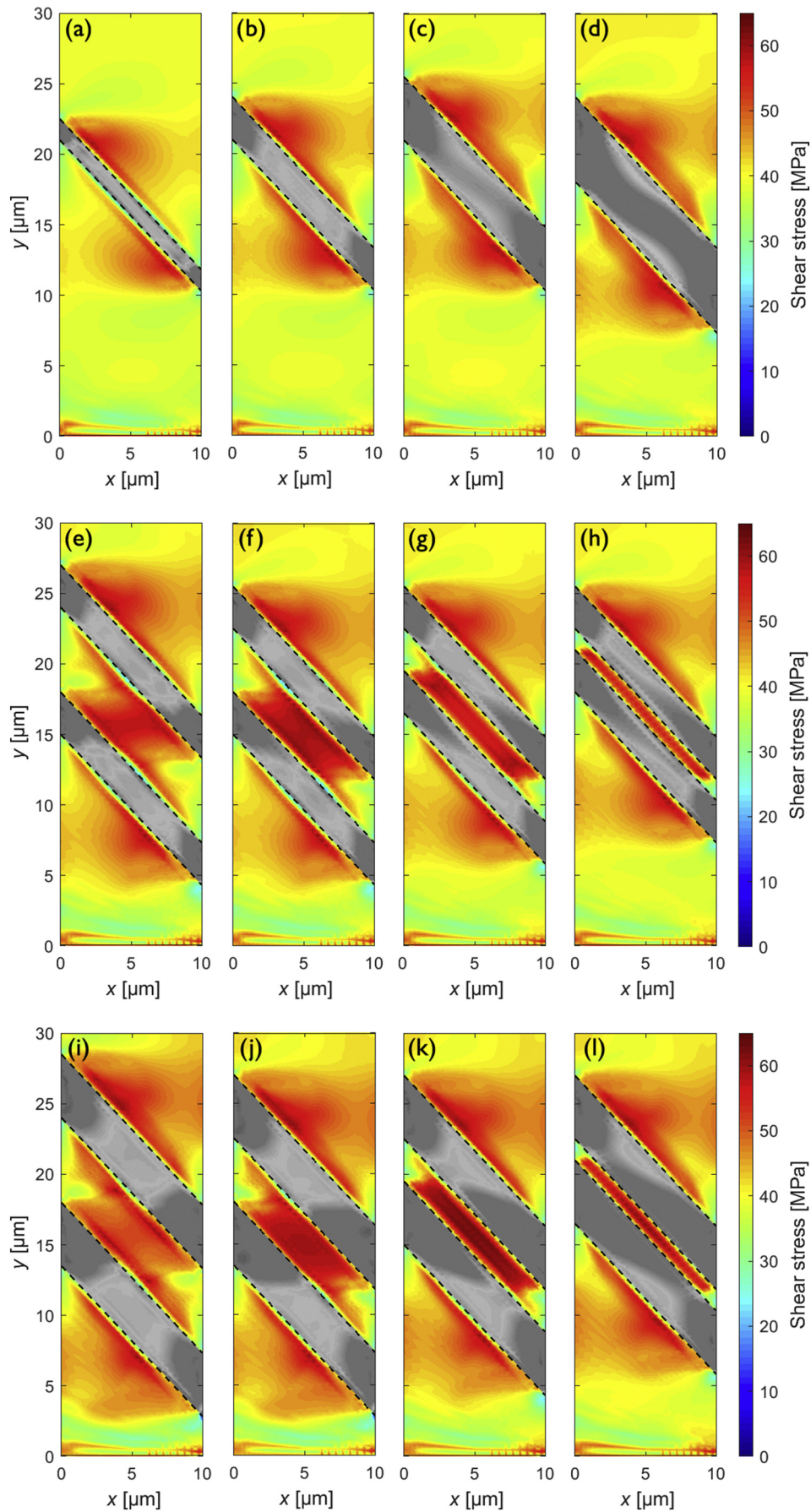


**Fig. 4.** The shear stress distribution in the twinning plane calculated using the FE model for different twin configurations: (a-d) single twin with the thickness of 1.5  $\mu\text{m}$ , 3  $\mu\text{m}$ , 4.5  $\mu\text{m}$ , or 6  $\mu\text{m}$ , respectively; (e-h) two twins with the thickness of 3  $\mu\text{m}$  and the distances of 6  $\mu\text{m}$ , 4.5  $\mu\text{m}$ , 3  $\mu\text{m}$ , or 1.5  $\mu\text{m}$ , respectively; (i-l) two twins with the thickness of 4.5  $\mu\text{m}$  and the distances of 6  $\mu\text{m}$ , 4.5  $\mu\text{m}$ , 3  $\mu\text{m}$ , or 1.5  $\mu\text{m}$ , respectively.

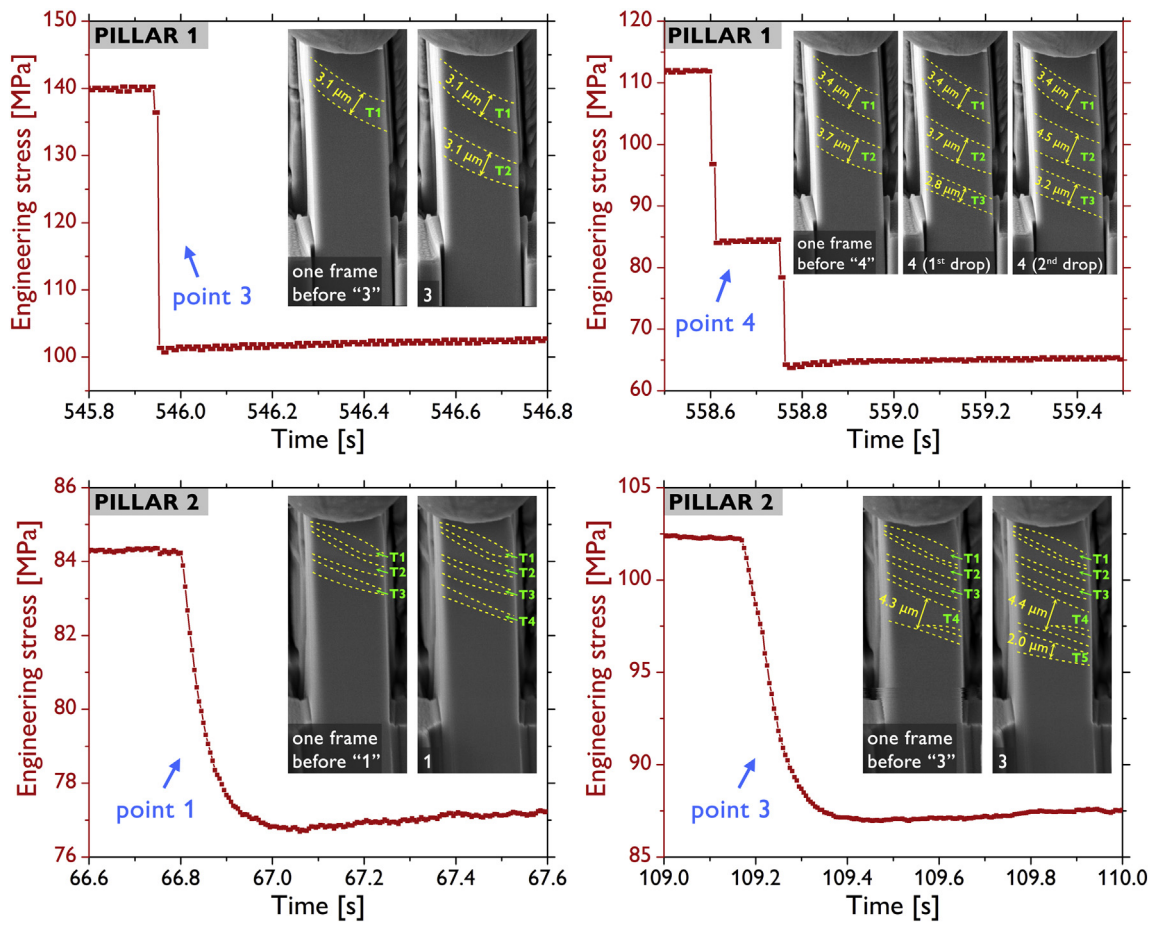


Fig. 5. Detailed view of the selected stress drops revealing twin nucleation and growth dynamics supplemented by respective SEM images.

investigated by Vinogradov et al. [32] using the acoustic emission experiments, which also showed highly correlated characteristics of twin formation. It must be, however, noted that bulk data can exhibit some differences due to strain multiaxiality.

Owing to the high sampling rate of the nano-testing device and the continuous SEM imaging approach, we were able to study the dynamics of twin nucleation at the early stage of its growth in great detail. In Fig. 5, we show four representative examples of stress drop events (two for

both tested pillars). Note that the indicated time interval on the x axis is the same (1 s) for each plot in Fig. 5, for the sake of easy comparison. Unexpectedly, we observed different initial thickening rates in the two pillars in terms of stress drops development. In pillar P1, the twins nucleated and grew in the initial stage very rapidly, see Fig. 5, P1 – points 3 and 4. The nucleation of each of these two twins (note that they correspond to T2 and T3 in P1 in Fig. 2 and 3) clearly manifests itself by significant stress drops associated with fast accommodation of the

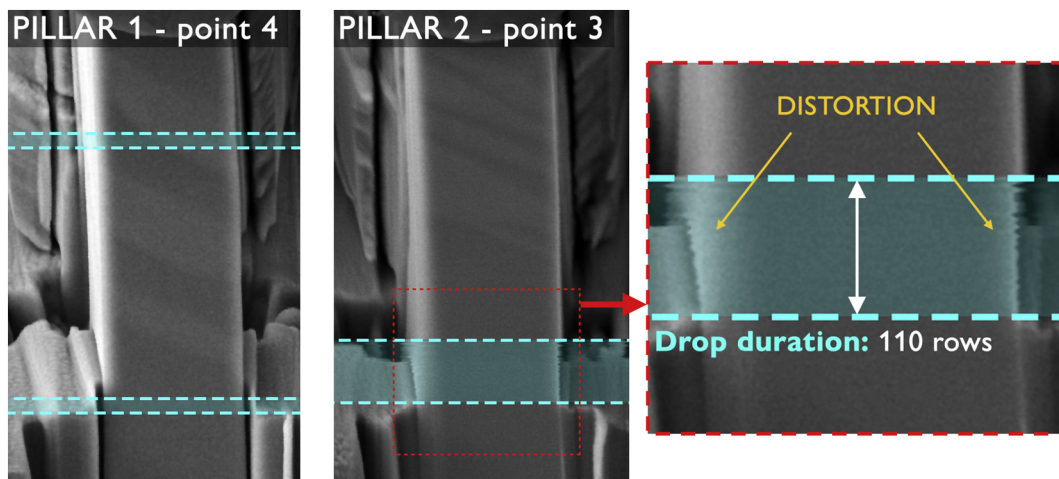


Fig. 6. The determination of the stress drop duration from distortions captured in the SEM images.

deformation. In other words, a newly developed twin effectively decreases the length of the pillar, which was detected as a sudden reduction in the applied force. The duration of the stress drops in the case of P1 was close to the sampling rate (200 points/s). Such a relatively high sampling rate allowed us to calculate quite precisely the values of the lateral growth rate. Twins in P1 nucleated and grew to the thickness of approximately 2–3  $\mu\text{m}$  within 0.01 s. Hence, this gives an estimation of the lower bound for the initial thickening rate in P1 of 2–3  $\cdot 10^{-4}$  m/s. A rather unusual intermittent initial growth dynamics were observed in the case of T4 in P1 (point 4). The initial stage of T4 nucleation was divided into two separate steps. The duration of both drops was approximately 0.01 s and they were separated by a time interval of  $\sim 0.14$  s. During the first drop, the twin nucleated and quickly grew to a thickness of  $\sim 2.3$   $\mu\text{m}$ , showing the thickening rate of at least 2.3  $\cdot 10^{-4}$  m/s. During the second drop, the twin grew to the final thickness of 3.4  $\mu\text{m}$ , yielding a thickening rate of at least 1.1  $\cdot 10^{-4}$  m/s.

On the other hand, the stress drops in the case of P2 took a much longer time of  $\sim 0.10$ – $0.15$  s, see Fig. 5. The kinetics of the twin growth exhibited rather transient characteristics with an “exponentially decaying” growth rate in terms of the observed shapes of load drops. The thickness of T4 and T5 in P2 after nucleation and initial growth was  $\sim 1.5$   $\mu\text{m}$  and  $\sim 2$   $\mu\text{m}$ , respectively, yielding the estimated initial thickening rate of roughly 1–1.5  $\cdot 10^{-5}$   $\mu\text{m/s}$ . We speculate that the dissimilarities in the twin nucleation and growth dynamics, as observed in Fig. 5, might be related to the fact that there were three pre-existing twins in P2. As discussed above, these twins could reduce the critical nucleation stress for further twin formation. This is in line with the observation that practically all the twins in P2 nucleated within the first  $\sim 170$  s while in the case of P1 the nucleation of new twins took place up to several hundreds of seconds (compare P1 and P2 in Figs. 1, 2, and 3). On the other hand, large back-stress imposed on these new twins in P2 retarded their lateral growth [7]. Another possible contribution to the observed dissimilarities might be a slight difference in the geometrical orientation of both pillars – P1 was slightly more prone to tilting during loading (this is best seen in the Supplementary videos), while P2 was being deformed almost parallel to the vertical axis with only minimal bending at earlier stages of the test. It was shown by Della Ventura et al. [20] that the orientation misfit as low as 5° could bring about significant differences in the micropillar deformation behavior. By any means, the occurrence of different deformation dynamics in the otherwise very similar micropillars is an interesting and non-trivial subject, and further detailed inquiry will be required to elucidate its origin.

The investigations of twin growth rates date back several decades [33] and the attempts to precisely measure the nucleation and propagation velocities, which are believed to approach the speed of sound in a material, still continue [34,35]. It must be, however, reminded that in this study, only the lateral growth rates (i.e. the twin thickening) were accessible due to the character of the tests. It was shown by Jeong et al. that even a frame rate of 25  $\text{s}^{-1}$  was insufficient to record nucleation and initial twin front propagation in Mg micropillars [18]. Nonetheless, our results confirmed that lateral twin growth is an arguably slower process than nucleation, as we were not able to capture any twin in the process of propagation across the pillar thickness.

We were additionally able to independently confirm the growth dynamics results deduced from the compression curves by a careful analysis of the SEM images. During twin nucleation, we were in most cases able to observe a significant jerky movement of the indenter tip, pillar, and a slight spring-back of the base material around the pillar. Realizing that the SEM image is generated point-by-point and knowing the exact dwell time of the electron beam for each pixel, we could use these images to detect processes with a time resolution better than 0.005 s. If the twin nucleation happened to take place during image acquisition, we could detect the exact moment of twin nucleation from the “shift” in the image and estimate its duration by comparing the image taken before and after twin nucleation (or, sometimes, even within a single

image). The distorted regions during compression of P2 were larger and easily discernible, thus corresponding well to the slower thickening rate of the twins. The stress drop relics in the SEM images were somewhat less discernible in the case of P1, where the drop dynamics were at least one order of magnitude faster. Nevertheless, we were still able to recognize several such events. One such example for each pillar is presented in Fig. 6. Two SEM image distortions were identified in P1 corresponding to the two-step nucleation and growth of T3 in P1 (point 4) – see Figs. 1, 2, and 4. Both distortions were visible in the range of  $\sim 30$  rows. The horizontal image resolution was 1024 pixels and the dwell time for each pixel was 0.3  $\mu\text{s}$ . Taken together, this gives an estimation of the drop duration of  $\sim 0.009$  s. The spatial difference between these two distortions was 410 lines, which (using the same rationale) gives the time separation of  $\sim 0.13$  s. Fig. 6 also shows the SEM image distortion brought about by the stress drop in P2 (T5) marked as “point 3” (see Figs. 1, 2, 3 and 5). Upon zooming in, this large distortion is well visible even in the static image, as seen in Fig. 6. This distortion “lasted”  $\sim 110$  image rows. The pixel dwell time for the SEM image acquisition for P2 was 1  $\mu\text{s}$ . In this case, the calculation gives an estimation of the drop duration of  $\sim 0.11$  s. All the estimated drop durations and drop separation duration are in excellent agreement with the durations determined from the deformation curves (Fig. 5). We will be further exploring the feasibility of these analyses with the aid of digital image correlation algorithms, which will be the subject of a separate follow-up study.

#### 4. Conclusions

Single-crystalline rectangular Mg micropillars (dimensions of  $10 \times 10 \times 30 \mu\text{m}^3$ ) having the orientation favorable for tensile twinning were fabricated using a novel method. The pillars were tested in compression using a high-precision nano-testing device with concurrent scanning electron microscopy imaging. The experimental data were supplemented by the finite element (FE) calculations. It was shown experimentally and also supported by FEM calculations that when the thickness of a single twin reaches a certain value (around 3  $\mu\text{m}$  for the studied micropillars), nucleation of further twin takes place, possibly accompanied with a certain thickening. This process is repeated until the twins form across the entire micropillar height, from its top to its base. Finally, the thickening and coalescence of all the twins take place until the whole volume of the micropillar is twinned. These observations can be effectively explained in terms of the FEM data, especially by means of the shear stress intensity and distribution. Using a line-by-line analysis of the SEM images together with a detailed examination of the compression curves (stress drops) allowed us also to effectively monitor twinning dynamics and to estimate the twin lateral growth rate in Mg micropillars to be on the order of  $10^{-5}$ – $10^{-4}$  m/s.

#### Data availability

The data that support the findings of this study are available from the authors upon reasonable request.

#### Credit author statement

**Kristián Máthís:** Conceptualization, Investigation, Supervision, Writing - Original Draft, Funding Acquisition. **Michal Knapék:** Data Curation, Validation, Writing - Review & Editing. **Filip Šiška:** Methodology, Software, Writing - Review & Editing. **Petr Hrcuba:** Methodology, Investigation, Data Curation. **Dávid Ugi:** Investigation, Visualization. **Péter Dušan Ispánovity:** Validation, Formal Analysis, Funding Acquisition. **István Groma:** Validation, Funding Acquisition, Resources. **Kwang Seon Shin:** Formal analysis, Supervision.

## Declaration of Competing Interest

The authors declare that they have no known competing financial interests or personal relationships that could have appeared to influence the work reported in this paper.

## Acknowledgments

FŠ and KM are grateful for the financial support from the Czech Science Foundation under the contract 18-07140S. MK acknowledges the financial support from the Operational Programme Research, Development and Education, The Ministry of Education, Youth and Sports (OP RDE, MEYS), grant No. CZ.02.1.01/0.0/0.0/16\_013/0001794. This work was completed within the ELTE Institutional Excellence Program (1783-3/2018/FEKUTSRAT) supported by the Hungarian Ministry of Human Capacities. DU, PDI and IG acknowledge the support of the National Research, Development and Innovation Fund of Hungary (contract numbers: NKFIH-K-119561, NKFIH-KH-125380).

## Appendix A. Supplementary data

Supplementary data to this article can be found online at <https://doi.org/10.1016/j.matdes.2021.109563>.

## References

- [1] P. Dobroň, F. Chmelík, S. Yi, K. Parfenenko, D. Letzig, J. Bohlen, Grain size effects on deformation twinning in an extruded magnesium alloy tested in compression, *Scr. Mater.* 65 (2011) 424–427, <https://doi.org/10.1016/j.scriptamat.2011.05.027>.
- [2] J. Čapek, M. Knappek, P. Minářík, J. Dittrich, K. Máthis, Characterization of deformation mechanisms in Mg alloys by advanced acoustic emission methods, *Metals* 8 (2018) 644, <https://doi.org/10.3390/met8080644>.
- [3] K. Máthis, K. Nyilas, A. Axt, I. Dragomir-Cernatescu, T. Ungar, P. Lukac, The evolution of non-basal dislocations as a function of deformation temperature in pure magnesium determined by X-ray diffraction, *Acta Mater.* 52 (2004) 2889–2894, <https://doi.org/10.1016/j.actamat.2004.02.034>.
- [4] A. Chapuis, J.H. Driver, Temperature dependency of slip and twinning in plane strain compressed magnesium single crystals, *Acta Mater.* 59 (2011) 1986–1994, <https://doi.org/10.1016/j.actamat.2010.11.064>.
- [5] J. Čapek, K. Máthis, B. Clausen, J. Stráská, P. Beran, P. Lukáš, Study of the loading mode dependence of the twinning in random textured cast magnesium by acoustic emission and neutron diffraction methods, *Mater. Sci. Eng. A* 602 (2014) 25–32, <https://doi.org/10.1016/j.msea.2014.02.051>.
- [6] X. Ma, Q. Jiao, L.J. Kecskes, J.A. El-Awady, T.P. Weihs, Effect of basal precipitates on extension twinning and pyramidal slip: a micro-mechanical and electron microscopy study of a Mg–Al binary alloy, *Acta Mater.* 189 (2020) 35–46, <https://doi.org/10.1016/j.actamat.2020.02.037>.
- [7] Y. Liu, N. Li, M. Arul Kumar, S. Pathak, J. Wang, R.J. McCabe, N.A. Mara, C.N. Tomé, Experimentally quantifying critical stresses associated with basal slip and twinning in magnesium using micropillars, *Acta Mater.* 135 (2017) 411–421, <https://doi.org/10.1016/j.actamat.2017.06.008>.
- [8] P. Zhang, O.U. Salman, J.-Y. Zhang, G. Liu, J. Weiss, L. Truskinovsky, J. Sun, Taming intermittent plasticity at small scales, *Acta Mater.* 128 (2017) 351–364, <https://doi.org/10.1016/j.actamat.2017.02.039>.
- [9] Q. Yu, Z.-W. Shan, J. Li, X. Huang, L. Xiao, J. Sun, E. Ma, Strong crystal size effect on deformation twinning, *Nature* 463 (2010) 335–338, <https://doi.org/10.1038/nature08692>.
- [10] M.D. Uchic, D.M. Dimiduk, A methodology to investigate size scale effects in crystal-line plasticity using uniaxial compression testing, *Mater. Sci. Eng. A* 400–401 (2005) 268–278, <https://doi.org/10.1016/j.msea.2005.03.082>.
- [11] M.D. Uchic, P.A. Shade, D.M. Dimiduk, Plasticity of micrometer-scale single crystals in compression, *Annu. Rev. Mater. Res.* 39 (2009) 361–386, <https://doi.org/10.1146/annurev-matsci-082908-145422>.
- [12] W.C. Crone, A brief introduction to MEMS and NEMS, in: W.N. Sharpe (Ed.), *Springer Handb. Exp. Solid Mech.* Springer US, Boston, MA 2008, pp. 203–228, [https://doi.org/10.1007/978-0-387-30877-7\\_9](https://doi.org/10.1007/978-0-387-30877-7_9).
- [13] L. Wang, Z. Zhang, X. Han, In situ experimental mechanics of nanomaterials at the atomic scale, *NPG Asia Mater.* 5 (2013) e40, <https://doi.org/10.1038/am.2012.70>.
- [14] M.D. Uchic, Sample dimensions influence strength and crystal plasticity, *Science* 305 (2004) 986–989, <https://doi.org/10.1126/science.1098993>.
- [15] W.L. Chan, M.W. Fu, J. Lu, The size effect on micro deformation behaviour in micro-scale plastic deformation, *Mater. Des.* 32 (2011) 198–206, <https://doi.org/10.1016/j.matdes.2010.06.011>.
- [16] J. Weiss, L. Girard, F. Gimbert, D. Amirano, D. Vandembroucq, (Finite) statistical size effects on compressive strength, *Proc. Natl. Acad. Sci.* 111 (2014) 6231–6236, <https://doi.org/10.1073/pnas.1403500111>.
- [17] W. Wang, Y. Zhong, K. Lu, L. Lu, D.L. McDowell, T. Zhu, Size effects and strength fluctuation in nanoscale plasticity, *Acta Mater.* 60 (2012) 3302–3309, <https://doi.org/10.1016/j.actamat.2012.03.016>.
- [18] J. Jeong, M. Alfreider, R. Konetschnik, D. Kiener, S.H. Oh, In-situ TEM observation of {101 $\bar{2}$ } twin-dominated deformation of mg pillars: twinning mechanism, size effects and rate dependency, *Acta Mater.* 158 (2018) 407–421, <https://doi.org/10.1016/j.actamat.2018.07.027>.
- [19] R. Chen, S. Sandlöbes, C. Zehnder, X. Zeng, S. Korte-Kerzel, D. Raabe, Deformation mechanisms, activated slip systems and critical resolved shear stresses in an mg-LPSO alloy studied by micro-pillar compression, *Mater. Des.* 154 (2018) 203–216, <https://doi.org/10.1016/j.matdes.2018.05.037>.
- [20] N.M. Della Ventura, S. Kalácska, D. Casari, T.E.J. Edwards, A. Sharma, J. Michler, R. Logé, X. Maeder, { 101 $\bar{2}$  } twinning mechanism during in situ micro-tensile loading of pure Mg: role of basal slip and twin-twin interactions, *Mater. Des.* 197 (2021) 109206, <https://doi.org/10.1016/j.matdes.2020.109206>.
- [21] J. Wang, N. Stanford, Investigation of precipitate hardening of slip and twinning in Mg5Zn by micropillar compression, *Acta Mater.* 100 (2015) 53–63, <https://doi.org/10.1016/j.actamat.2015.08.012>.
- [22] J. Wang, J.M. Molina-Aldareguia, J. Llorca, Effect of Al content on the critical resolved shear stress for twin nucleation and growth in Mg alloys, *Acta Mater.* 188 (2020) 215–227, <https://doi.org/10.1016/j.actamat.2020.02.006>.
- [23] H. Fei, A. Abraham, N. Chawla, H. Jiang, Evaluation of micro-pillar compression tests for accurate determination of elastic-plastic constitutive relations, *J. Appl. Mech.* 79 (2012), 061011, <https://doi.org/10.1115/1.4006767>.
- [24] B. Kondori, A. Needleman, A. Amine Benzerga, Discrete dislocation simulations of compression of tapered micropillars, *J. Mech. Phys. Solids* 101 (2017) 223–234, <https://doi.org/10.1016/j.jmps.2017.01.015>.
- [25] G.-D. Sim, K.Y. Xie, K.J. Hemker, J.A. El-Awady, Effect of temperature on the transition in deformation modes in Mg single crystals, *Acta Mater.* 178 (2019) 241–248, <https://doi.org/10.1016/j.actamat.2019.08.014>.
- [26] Á.I. Hegyi, P.D. Ispánovity, M. Knappek, D. Túzes, K. Máthis, F. Chmelík, Z. Dankházi, G. Varga, I. Groma, Micron-scale deformation: a coupled in situ study of strain bursts and acoustic emission, *Microsc. Microanal.* (2017) 1–6, <https://doi.org/10.1017/S1431927617012594>.
- [27] T.R. Long, C.S. Smith, Single-crystal elastic constants of magnesium and magnesium alloys, *Acta Metall.* 5 (1957) 200–207, [https://doi.org/10.1016/0001-6160\(57\)90166-9](https://doi.org/10.1016/0001-6160(57)90166-9).
- [28] J. Mandel, Equations constitutives et directeurs dans les milieux plastiques et viscoplastiques, *Int. J. Solids Struct.* 9 (1973) 725–740, [https://doi.org/10.1016/0020-7683\(73\)90120-0](https://doi.org/10.1016/0020-7683(73)90120-0).
- [29] R.J. Asaro, Crystal plasticity, *J. Appl. Mech.* 50 (1983) 921–934, <https://doi.org/10.1115/1.3167205>.
- [30] C. Guillemer, M. Clavel, G. Cailletaud, Cyclic behavior of extruded magnesium: experimental, microstructural and numerical approach, *Int. J. Plast.* 27 (2011) 2068–2084, <https://doi.org/10.1016/j.ijplas.2011.06.002>.
- [31] M. Arul Kumar, A.K. Kanjarla, S.R. Niezgodna, R.A. Lebensohn, C.N. Tomé, Numerical study of the stress state of a deformation twin in magnesium, *Acta Mater.* 84 (2015) 349–358, <https://doi.org/10.1016/j.actamat.2014.10.048>.
- [32] A. Vinogradov, E. Agletdinov, D. Merson, Mechanical twinning is a correlated dynamic process, *Sci. Rep.* 9 (2019) 5748, <https://doi.org/10.1038/s41598-019-42317-4>.
- [33] A.H. Cottrell, B.A. Bilby, A mechanism for the growth of deformation twins in crystals, *Lond. Edinb. Dublin Philos. Mag. J. Sci.* 42 (1951) 573–581, <https://doi.org/10.1080/14786445108561272>.
- [34] P. Rosakis, H. Tsai, Dynamic twinning processes in crystals, *Int. J. Solids Struct.* 32 (1995) 2711–2723, [https://doi.org/10.1016/0020-7683\(94\)00293-6](https://doi.org/10.1016/0020-7683(94)00293-6).
- [35] A. Vinogradov, E. Vasilev, M. Seleznev, K. Máthis, D. Orlov, D. Merson, On the limits of acoustic emission detectability for twinning, *Mater. Lett.* 183 (2016) 417–419, <https://doi.org/10.1016/j.matlet.2016.07.063>.